

Inductive electric fields in the inner magnetosphere during geomagnetically active periods

S. Ohtani,¹ H. Korth,¹ K. Keika,² Y. Zheng,^{1,3} P. C. Brandt,¹ and S. B. Mende⁴

Received 31 May 2010; revised 20 July 2010; accepted 11 August 2010; published 18 December 2010.

[1] The present study examines the characteristics of electric fields in the nightside inner magnetosphere during geomagnetically active periods. Electric field and magnetic field measurements made by the Cluster spacecraft on their perigee passes are used. The results are summarized as follows: (1) The duskward electric field component E_Y tends to be larger in the premidnight sector and off the equator, presumably corresponding to the more frequent occurrence of substorms and boundary layer crossings, respectively. (2) The occurrence distribution of E_Y is biased positively with an average of 0.6–0.8 mV/m, which reflects enhanced convection at active time. (3) The occurrence distribution of E_Y is also characterized by extending tails with a standard deviation larger than the twice the average. Although the occurrence ratio decreases sharply with increasing magnitude of E_Y , $|E_Y|$ occasionally exceeds 5 mV/m. (4) The sign of E_Y is well organized by the change of magnetic field. When the local magnetic configuration becomes more dipolar, E_Y tends to be positive (duskward), whereas it tends to be negative (dawnward) when the configuration becomes more stretched. (5) As for strong electric fields, E_Y tends to be proportional to the change of the H magnetic component, and from the induction equation, the typical spatial scale of E_Y is estimated at $4.2 R_E$. Results 4 and 5 strongly suggests that those strong electric fields are inductive. However, the corresponding process/phenomenon can be different from event to event. It is also suggested that substorm(-like) processes inside the ring current effectively intensify the ring current.

Citation: Ohtani, S., H. Korth, K. Keika, Y. Zheng, P. C. Brandt, and S. B. Mende (2010), Inductive electric fields in the inner magnetosphere during geomagnetically active periods, *J. Geophys. Res.*, 115, A00I14, doi:10.1029/2010JA015745.

1. Introduction

[2] The energization and transport of ring current ions are determined primarily by electric field in the near-Earth magnetosphere. With increasing solar wind-magnetosphere coupling, the cross-polar cap potential increases [e.g., Reiff *et al.*, 1981] and the electric field becomes stronger in the inner magnetosphere [Maynard *et al.*, 1983; Rowland and Wygant, 1998; Wygant *et al.*, 1998; Nishimura *et al.*, 2006]. For example, at $L = 4\sim 5$, the average duskward electric field is about 1 mV/m for $Kp > 5$, whereas it is of the order of one tenth of 1 mV/m for $Kp < 3$ [Rowland and Wygant, 1998]. If it is static, an electric field of 1 mV/m corresponds to a 130 kV potential difference over $20 R_E$, which is close to the maximum potential difference across the polar cap [e.g., Shepherd *et al.*, 2002].

[3] However, the electric field in the inner magnetosphere is highly variable and occasionally becomes much larger than 1 mV/m [e.g., Maynard *et al.*, 1983; Wygant *et al.*, 1998]. During the April 2002 storm event, for example, large electric field (a few tens of mV/m) fluctuations were observed inside the ring current ($< 4.6 R_E$) [Ohtani *et al.*, 2007; hereafter Paper 1]. Such strong electric fields must be temporal or spatially localized because otherwise the associated potential difference would be unrealistically large. The convection in the near-Earth plasma sheet is also bursty at storm time [Hori *et al.*, 2005; Ohtani and Mukai, 2008] as well as at nonstorm time [Angelopoulos *et al.*, 1992]. Therefore, it seems that in both the plasma sheet and the ring current, the convection is rather impulsive and is far from steady.

[4] The impulsive electric field is often associated with substorm activity, and its role in the storm time ring current formation (intensification) has been one of the most controversial issues of storm dynamics [e.g., Gonzalez *et al.*, 1994; Kamide *et al.*, 1998; Daglis *et al.*, 1999; Ebihara and Ejiri, 2003]. The issue is difficult to address observationally with limited spatial coverage of spacecraft in the magnetosphere, and the results of modeling efforts are not conclusive [Chen *et al.*, 1994; Fok *et al.*, 1996, 1999; Ebihara and Ejiri, 2003]. It has also been suggested that the enhancement of magnetospheric convection is the primary cause of the ring

¹Johns Hopkins University Applied Physics Laboratory, Laurel, Maryland, USA.

²Center for Solar-Terrestrial Research, New Jersey Institute of Technology, Newark, New Jersey, USA.

³NASA Goddard Space Flight Center, Greenbelt, Maryland, USA.

⁴Space Sciences Laboratory, University of California, Berkeley, California, USA.

current intensification [e.g., *Wolf et al.*, 1997; *McPherron*, 1997].

[5] In general the area of closed drift orbits shrinks as the convection strengthens, and particles transported from the plasma sheet eventually exit from the dayside magnetopause as far as the convection is steady. Such particles may contribute to the formation and intensification of a partial ring current, but the effect of each convection enhancement would be temporary. In contrast, if the electric field, whether related to a substorm or not, strengthens transiently around the nightside boundary of the closed-orbit area, it may most effectively transport fresh particles into the ring current. In addition, strong electric fields inside the closed-orbit region bring particles deeper into the ring current on the nightside and at the same time they energize those particles. However, despite such potentially critical importance for better understanding the storm time ring current dynamics, the nature of electric fields in the inner magnetosphere still remains to be understood.

[6] In the present study we examine the characteristics of electric fields in the nightside inner magnetosphere during geomagnetically active periods. Cluster electric field and magnetic field data are used as a primary data set. In section 2 we briefly describe our data set. In section 3 we examine the 18 January 2005 storm event as an example. The statistical characteristics of electric fields are examined in section 4. Results are discussed in section 5. Section 6 is a summary.

2. Cluster Data Set

[7] In the present study we use electric field and magnetic field measurements made by the Cluster satellites as a primary data set. The Cluster mission [*Escoubet et al.*, 2001] consists of four identical satellites, which fly in formation with variable separation distances ranging from a few hundred kilometers to a few R_E . The spacecraft were launched in August 2000. Its $4 \times 19 R_E$ orbit has a high inclination angle, 90° , and therefore, the spacecraft cross the equatorial plane almost vertically. The spin axis of each satellite is approximately perpendicular to the ecliptic plane, and the spin period is 4 s.

[8] The electric fields and waves (EFW) instrument [*Gustafsson et al.*, 2001] measures the electric field in the spacecraft spin plane, which is approximately parallel to the GSE X - Y plane. In this study we use the Y component of the spin averages E_Y , which is positive toward dusk. The induction electric field due to the satellite motion is removed. Data were provided by the Cluster Active Archive along with quality flag, and we use measurements qualified as “3,” which is next only to visually validated measurements, or as “2” only because of precaution for the simultaneous active mode operation of the WHISPER instrument, which transmits radio waves for topside sounding.

[9] We also use spin-averaged (4 s) magnetic field measurements made by the fluxgate magnetometer [*Balogh et al.*, 2001]. Because our focus is on the inner magnetosphere, where the terrestrial dipole field is dominant, we adopt the VDH coordinate system. In this coordinate system H is parallel to the dipole axis and is positive northward, V points radially outward and is parallel to the magnetic equator, and D completes a right-hand orthogonal system and is positive eastward.

[10] For the event study (section 3) we use auroral UVI and energetic neutral atom (ENA) images taken by the WIC [*Mende et al.*, 2000] and HENA [*Mitchell et al.*, 2000] instruments, respectively, onboard the IMAGE satellite [*Burch*, 2000]. Interplanetary magnetic field (IMF) and solar wind data were obtained from the MAG [*Smith et al.*, 1998] and Solar Wind Electron Proton Alpha Monitor [*McComas et al.*, 1998] instruments, respectively, onboard the ACE satellite at the L1 point.

3. The 18 January 2005 Event

[11] In this section we examine a storm event of 18 January 2005 with a focus on Cluster measurements on its perigee pass in the postmidnight sector. We chose this event as an example for the following four reasons. First, the Cluster constellation passed the magnetic equator around the time of the Sym - H minimum. Second, the quality of the spin-averaged Cluster/EFW measurements was excellent throughout the perigee pass. Third, IMAGE/WIC auroral images are available for this event, which allows addressing global auroral activity. Finally, this event took place when Cluster was in the postmidnight sector, whereas in a previously reported event, the April 2002 storm event, it was located in the premidnight sector [Paper 1].

[12] Figure 1 shows, from the top, the IMF B_Z component, the solar wind dynamic pressure, the Sym - H and Asy - H indices, and the AU and AL indices for the 8 h interval centered at 0200 UT on 18 January 2005. The vertical dotted line marks 0120 UT, when the initial auroral intensification was identified as will be shown later. The IMF and solar wind data were acquired by the ACE satellite and were time shifted to 1 AU from its L1 position. IMF B_Z changed from strongly positive (>10 nT) to strongly negative (<-10 nT) around ~ 2340 UT on the previous day. Responding to this southward turning of IMF B_Z , Sym - H decreased sharply reaching below -50 nT just before the day boundary, and auroral electrojets also developed. IMF B_Z remained <-10 nT until 0125 UT, when it became positive transiently. During the same interval, Sym - H decreased reaching its minimum, -89 nT, slightly before the transient northward turning.

[13] It appears that the start of the Sym - H recovery was associated with a sharp increase in the solar wind dynamic pressure. In fact, the time profile of Sym - H resembles that of the dynamic pressure. On the dayside, the ground H component at Kakioka (magnetic latitude [MLat] = 27.7° and LT = 10.7; not shown) started to increase at 0120 UT presumably responding to the enhancement of the solar wind dynamic pressure. Note also that the start of the Sym - H recovery coincided with the start of the auroral intensification, which was immediately followed by a sharp decrease of AL and also by an increase of AU . The Asy - H index increased simultaneously with the enhancement of auroral electrojets, which is indicative of the intensification of field-aligned currents (FACs) or of the formation of a substorm FAC system. A substorm often takes place at the start of the (apparent) recovery of Sym - H [*Ohtani et al.*, 2001], and this event is another such example, although the effect of the solar wind dynamic pressure might dominate the effect of substorm-related tail current reduction in this event.

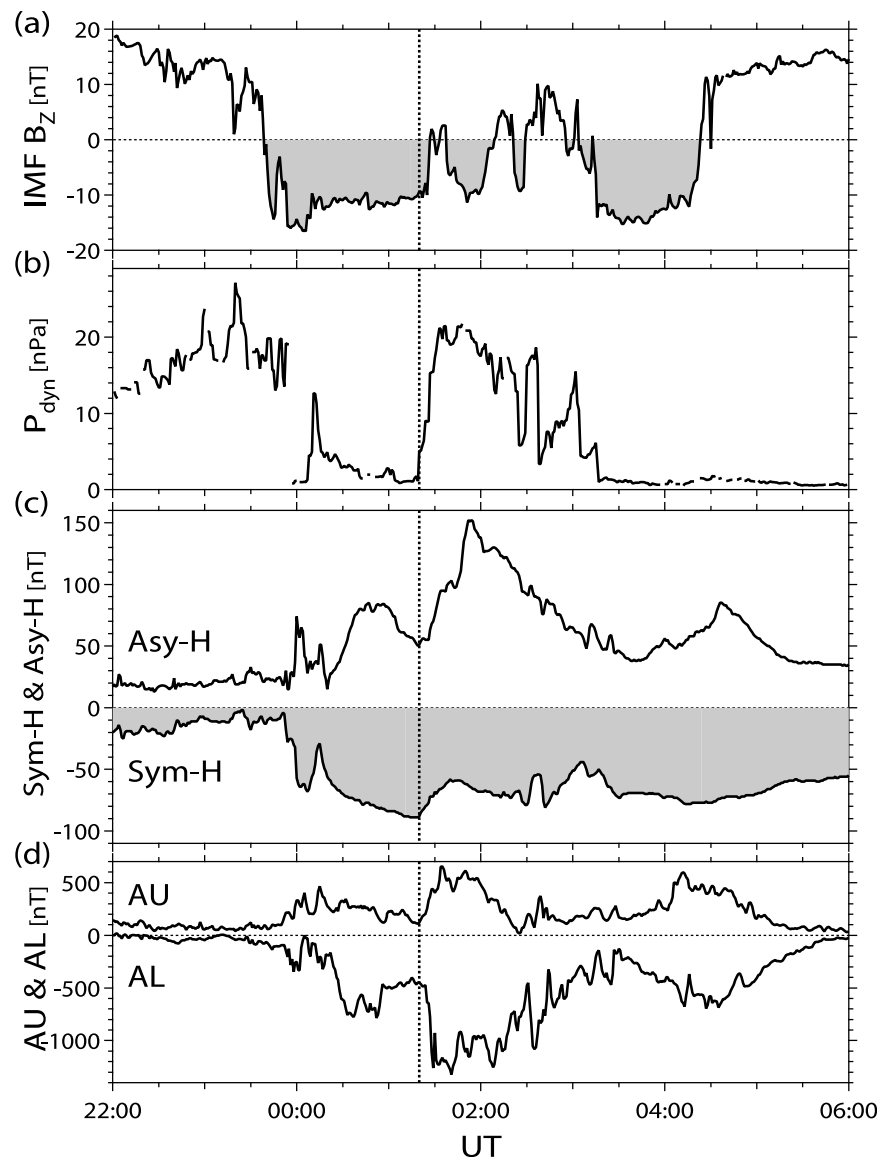


Figure 1. (a) IMF B_z , (b) solar wind dynamic pressure, (c) the *Sym-H* and *Asy-H* indices, and (d) the *AU* and *AL* indices for the 8 h interval from 2200 UT on 17 January 2005 to 0600 UT on 18 January. The IMF and solar wind data were acquired by the ACE satellite around the L1 point and are time shifted to 1 AU.

[14] Figures 2a and 2b show the orbit of Cluster 1 on 18 January 2005 in the SM X - Z and X - Y planes, respectively. The spacecraft was on a perigee pass moving from the Southern to the Northern Hemisphere crossing the magnetic equator (MLat = 0) at 0219 UT at MLT \sim 03. The perigee distance of Cluster is $4.0 R_E$. The period of interest is from 0110 to 0210 UT, during which all Cluster satellites were below the equator. The diagram inserted in Figures 2a and 2b shows the relative locations of the other Cluster satellites (identified by number) to Cluster 1 at 0140 UT. The scale factor for the interspacecraft separation in the plot is 2000 km per $1 R_E$. During this 1 h interval, Cluster 1 was closest to the magnetic equator and Cluster 3 was the farthest from it. The separation between these two satellites was $0.75 R_E$ in Z and 15 min in time. Cluster 2 was around the

middle of Clusters 1 and 3 in Z , and Cluster 4 was closest to Cluster 1 in both Z and MLT.

[15] Figure 3 plots three magnetic field components measured by Cluster 1 (solid lines) along with the quiet time ($K_p = 0$) T89 model field (dotted lines) [Tsyganenko, 1989] as a reference. The observation follows well the model field in each component. The sign of the V component changed at 0222 UT, a few minutes after the expected crossing of the magnetic equator, and the H component was close to its peak. The measured H component was depressed from the model field throughout the interval, which can be attributed to an intense ring current (outside of the Cluster location) and tail current. The intense ring current (in the radial distance range of Cluster) also explains the larger magnitude of the measured V component off the equator in the Southern

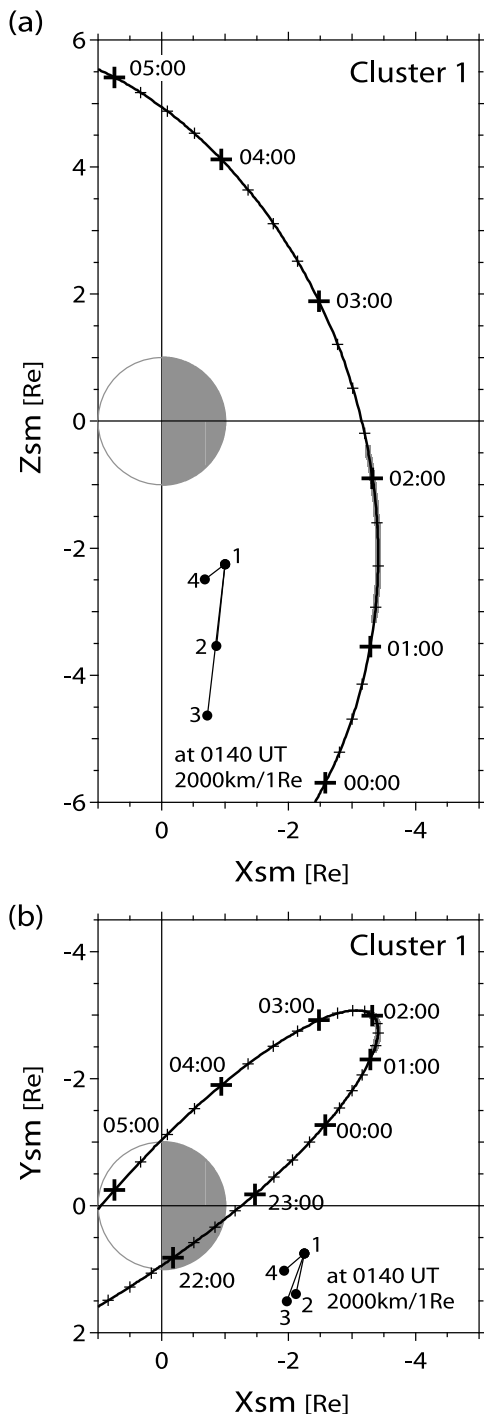


Figure 2. Positions of the Cluster 1 satellite along its perigee pass on 18 January 2005 in the (a) X - Z and (b) X - Y SM planes. The inserts show the relative locations of the other three Cluster satellites (as identified by the satellite numbers) to Cluster 1 at 0140 UT on a different scale ($2000 \text{ km}/1 R_p$).

Hemisphere. A better agreement in V in the Northern Hemisphere suggests that in the Cluster MLT sector the ring current was reduced in intensity around the time of the equatorial crossing. The D component was significantly smaller than the H or V component. That is, the magnetic

field lay approximately in the magnetic meridional plane throughout the interval.

[16] In Figure 3 many fluctuations are superposed on the background trend of each component especially before the crossing of the magnetic equator. In Figure 4 we plot each magnetic component after subtracting the model magnetic field. Here, data from all four Cluster satellites are shown in different colors. The horizontal axis ranges from 0110 to 0210 UT, the aforementioned 1 h interval. ΔV , the difference between the observed and model V components (the same notation applies to the other components, too), started to increase at 0120 UT at all Cluster satellites owing to the external compression. The local magnetic field was mostly in the V direction then (Figure 3), and therefore, the increase in V corresponds to an increase in the total field strength. Large magnetic fluctuations, especially in the D and H components, started at 0125 UT. Energetic ion and electron fluxes measured by the Cluster/RAPID instrument increased simultaneously (not shown). In all components, magnetic fluctuations were observed first by Clusters 1 and 4 closer to the magnetic equator, indicating that the associated structure expanded from equatorward.

[17] Another noticeable feature is a sharp increase in H at 0145 UT, which was observed by Clusters 1 and 4 but not by Cluster 2 or 3. ΔV , therefore $|V|$, too, decreased simultaneously. That is, the local magnetic field changed from a stressed to a more dipolar configuration. ΔD also decreased sharply. A similar decreases in D was observed ~ 5 min later at Cluster 2 and then another 5 min later at Cluster 3, suggesting a spatial structure passing the satellites relatively poleward. However, the corresponding signatures in the V and H components were noticeably smaller at those satellites than at Clusters 1 and 4. It is therefore unlikely that

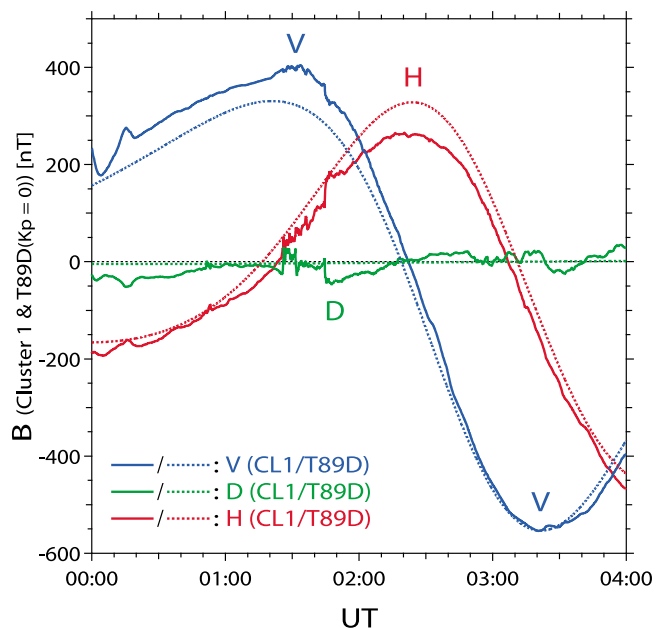


Figure 3. The V (blue), D (green), and H (red) magnetic components measured by Cluster 1 (solid) along with the T89 ($K_p = 0$) model field (dotted) at the Cluster 1 position for 0000–0400 UT on 18 January 2005.

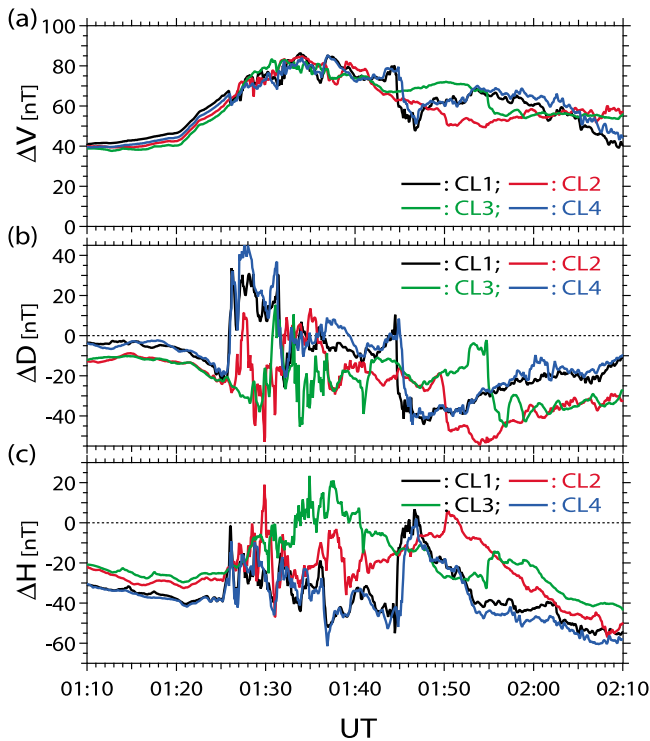


Figure 4. The (a) V , (b) D , and (c) H magnetic components measured by Cluster 1 (black), 2 (red), 3 (green), and 4 (blue) for 0100–0210 UT on 18 January 2005. The quiet time ($Kp = 0$) T89 model field is subtracted.

the same structure passed through all four satellites vertically. Alternatively, the difference among the satellites may be attributed to a longitudinal structure. Note that Clusters 1 and 4 were located slightly on the dawnside of Clusters 2 and 3 (Figure 2b). Provided that the dipolarization signature was propagating radially inward from Clusters 1 to 4, the propagation velocity is estimated from the satellite separation and the time delay of the dipolarization signature to be 30 km/s ($0.3 R_E/\text{min}$).

[18] Figure 5a plots ΔH (black line) and E_Y (red area) measured by Cluster 1 for the same 1 h interval. For 0125–0137 UT (marked by the blue horizontal bar), when the H component fluctuated largely, E_Y alternated its sign frequently, and its magnitude exceeded the range of the vertical axis several times. Whereas the variations of both ΔH and E_Y are highly irregular, ΔH and E_Y appear to be closely related. Figure 5b is a close-up of this 12 min interval. Although there are exceptions, in general, E_Y tends to be positive and negative when ΔH increases and decreases, respectively. The dipolarization of the local magnetic field at 0145 UT (Figure 5a) is another good example of this tendency. A large (>20 mV/m) E_Y peak is isolated in the middle of a period of relatively small E_Y , and its timing coincided with the sharp increase in the H component. We confirmed that Cluster 2, which did not observe any clear dipolarization signature, did not observe any similar enhancement of E_Y , either, around the time when Cluster 1 observed the large E_Y spike (not shown).

[19] Finally, it should be useful to address the Cluster observations in the context of global magnetospheric dynamics. Figure 6 shows global auroral images in the Southern Hemisphere taken by the IMAGE/WIC instrument

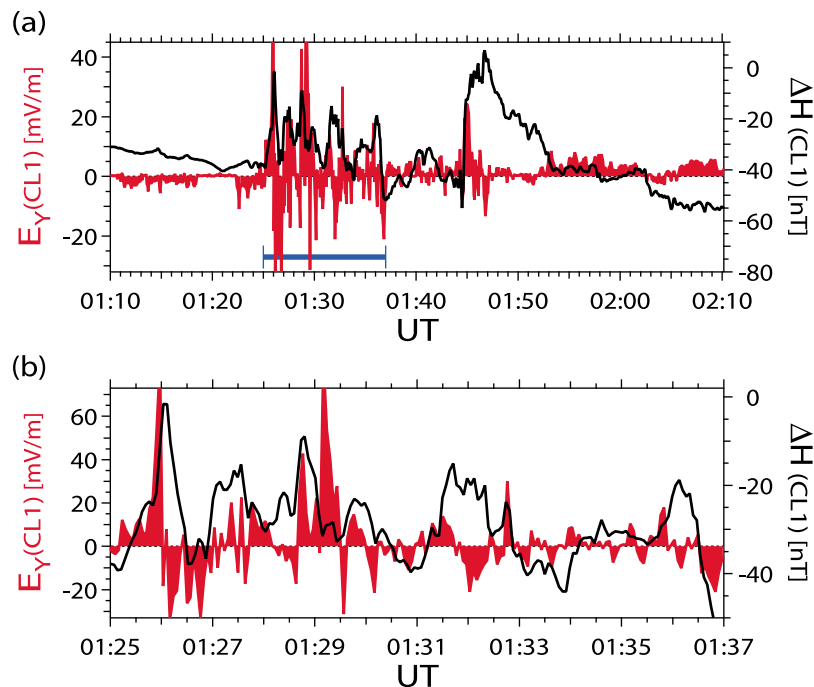


Figure 5. (a) E_Y (red area; labeled to the left) and ΔH (black line; labeled to the right), the difference between the measured and quiet time T89 model field, at Cluster 1 for 0100–0210 UT on 18 January 2005. (b) The same but for 0125–0137 UT, the interval shown by the blue horizontal bar in Figure 5a.

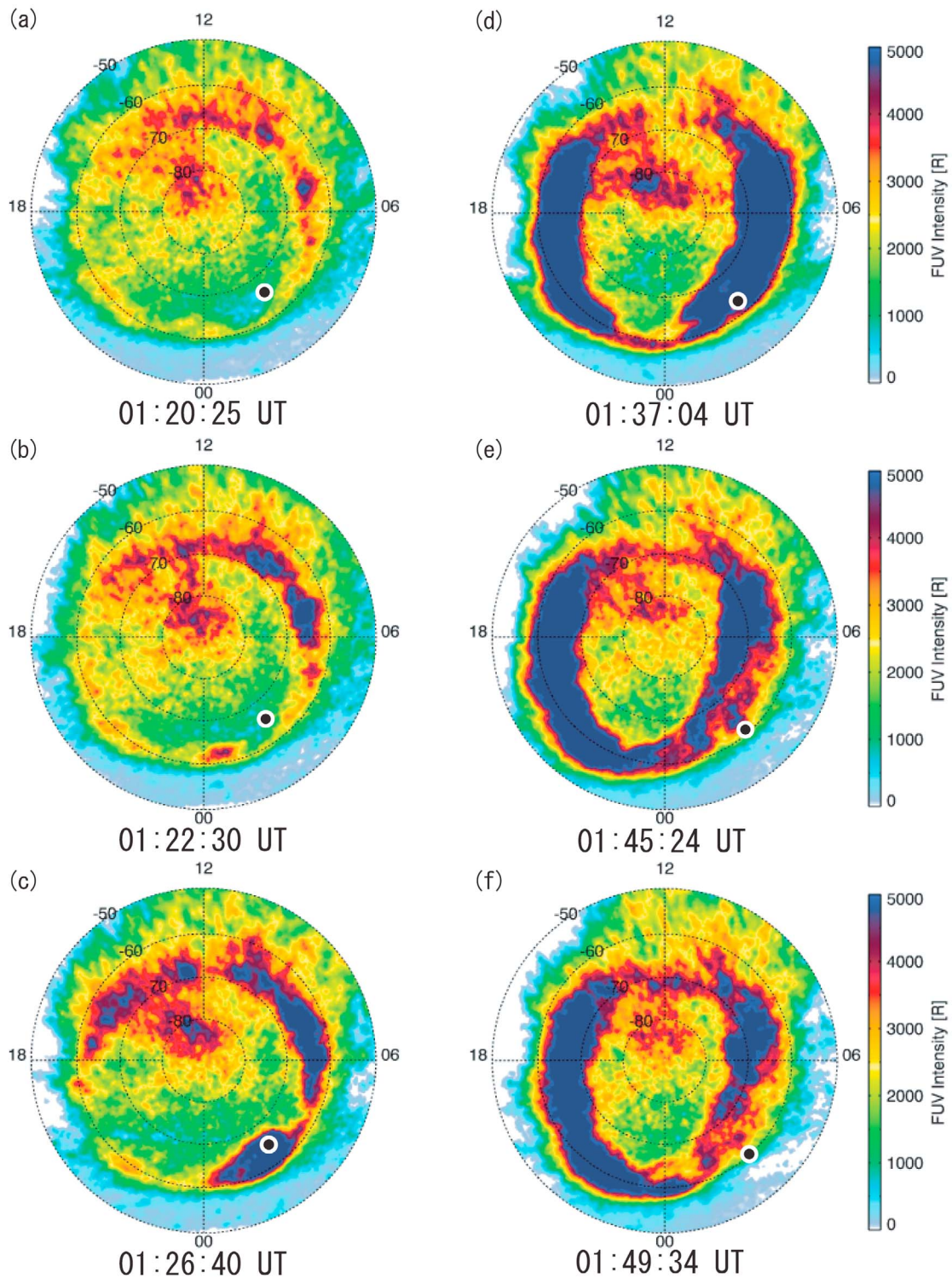


Figure 6. (a–f) Selected auroral images taken by IMAGE/WIC in the Southern Hemisphere on 18 January 2005. The foot point of Cluster 1 is shown by the white circle with a black solid circle in it in each panel.

at different times. The white circle with a solid black circle within it marks the magnetic footpoint of the Cluster 1 satellite calculated with the T96 model [Tsyganenko, 1996] with IMF $B_z = -10$ nT, IMF $B_y = 0$ nT, $Dst = -70$ nT, and a solar wind dynamic pressure of 15 nPa (here we assumed

that the magnetospheric configuration was still under the influence of the preceding strong southward IMF B_z , whereas the effect of the high dynamic pressure already arrived). The WIC instrument takes images with an exposure period of 24 s, and each frame is labeled with the start time of the

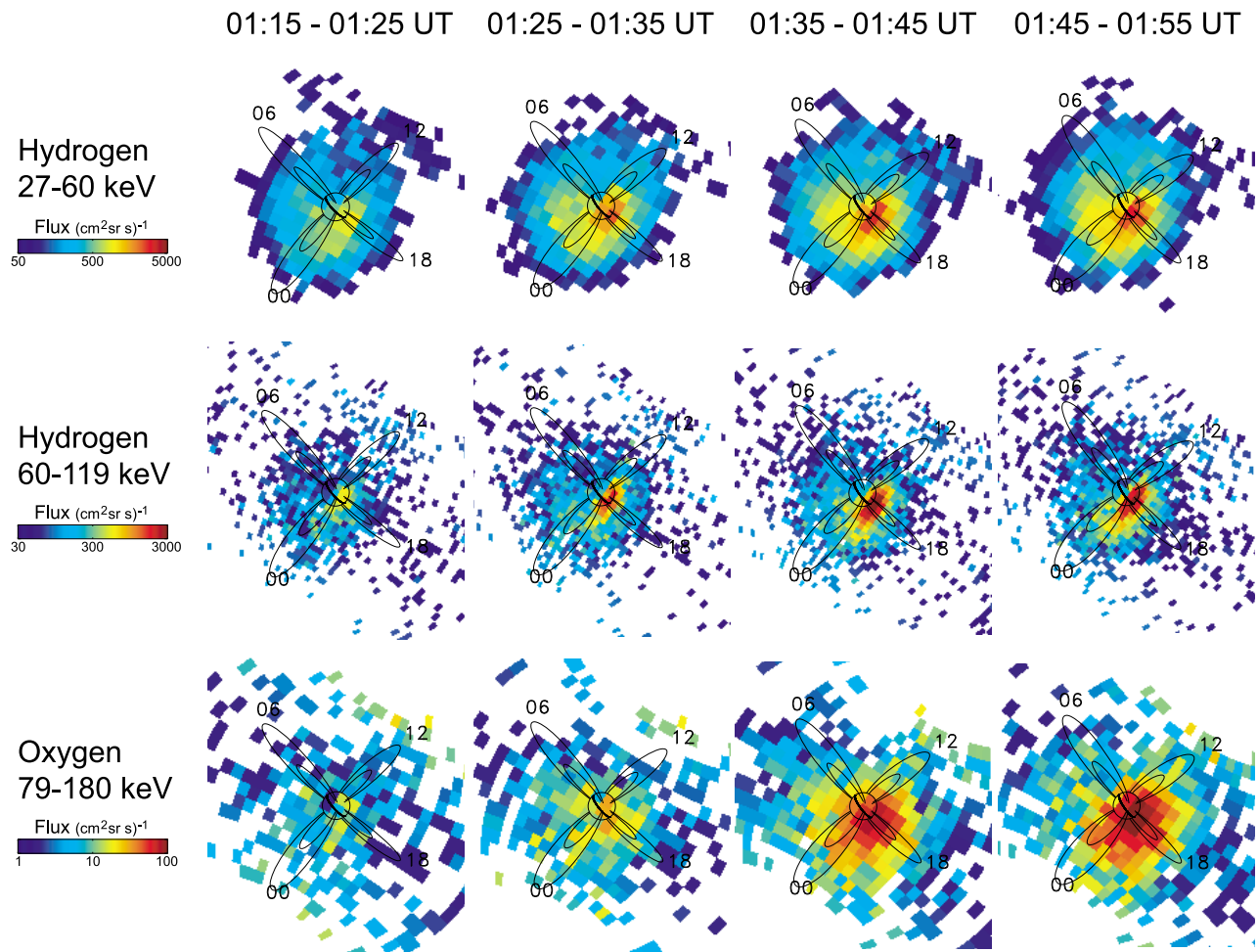


Figure 7. (top) Low-energy hydrogen (27–60 keV), (middle) high-energy hydrogen (60–119 keV), and (bottom) oxygen (79–180 keV) ENA images taken by IMAGE/HENA for four consecutive 10 min intervals from 0115 to 0155 UT on 18 January 2005. The circle at the center represents the Earth, and also shown are $L = 4$ and 8 dipole field lines at four local times. The IMAGE satellite was in the Southern Hemisphere moving from $(-1.5, -2.2, -7.7) R_E$ to $(-1.8, -2.8, -7.3) R_E$ in SM from 0115 to 0155 UT. Note that dawn is to the top left and dusk is to the bottom right.

exposure. At 0120:25 UT, a small bright spot appeared just after midnight slightly poleward of -60° in MLat (Figure 6a). This is the very initial signature of the subsequent substorm-like phenomenon. The timing coincided with the arrival of the enhanced solar wind dynamic pressure (Figure 1). It has been reported that aurora is activated on the nightside by solar wind compression after a period of strongly southward IMF B_z [e.g., Zhou and Tsurutani, 2001; Lyons et al., 2005; Keika et al., 2009]. In 2 min the bright spot intensified and expanded mostly eastward (Figure 6b). By 0126 UT, slightly after large magnetic fluctuations started at Cluster 1, the area of intense auroral emission expanded farther eastward and poleward swallowing the footpoint of Cluster (Figure 6c). This supports our interpretation that at the Cluster position the region of large magnetic fluctuations expanded from equatorward. At 0137 UT, the overall auroral activity was near its peak (Figure 6d). Interestingly, the global auroral distribution clearly shows two branches, one on the dawnside and another on the duskside, which is a pattern often observed during the substorm growth phase in association

with enhanced convection but usually with much weaker intensity [Shue et al., 2002]. The active auroral region that had expanded eastward from midnight merged with another active region expanding from dayside forming the dawnside branch. (This auroral morphology is the primary reason why we call this event substorm-like but not substorm.) Then the dawnside branch degraded, and at 0145UT when Clusters 1 and 4 observed the dipolarization, the satellite footpoint was just equatorward of a residual patch of auroral emission (Figure 6e). This is consistent with the fact that the dipolarization signature was localized in the magnetosphere. The degradation of the dawnside auroral branch proceeded even after the dipolarization at Cluster (Figure 6f). Obviously, the observed dipolarization made very little, if at all, impact on global auroral activity.

[20] The ENA measurement provides another insight about global magnetospheric dynamics of this event. Figure 7 shows low-energy hydrogen (27–60 keV; top), high-energy hydrogen (60–119 keV; middle), and oxygen (79–180 keV; bottom) ENA images taken by the IMAGE/HENA instru-

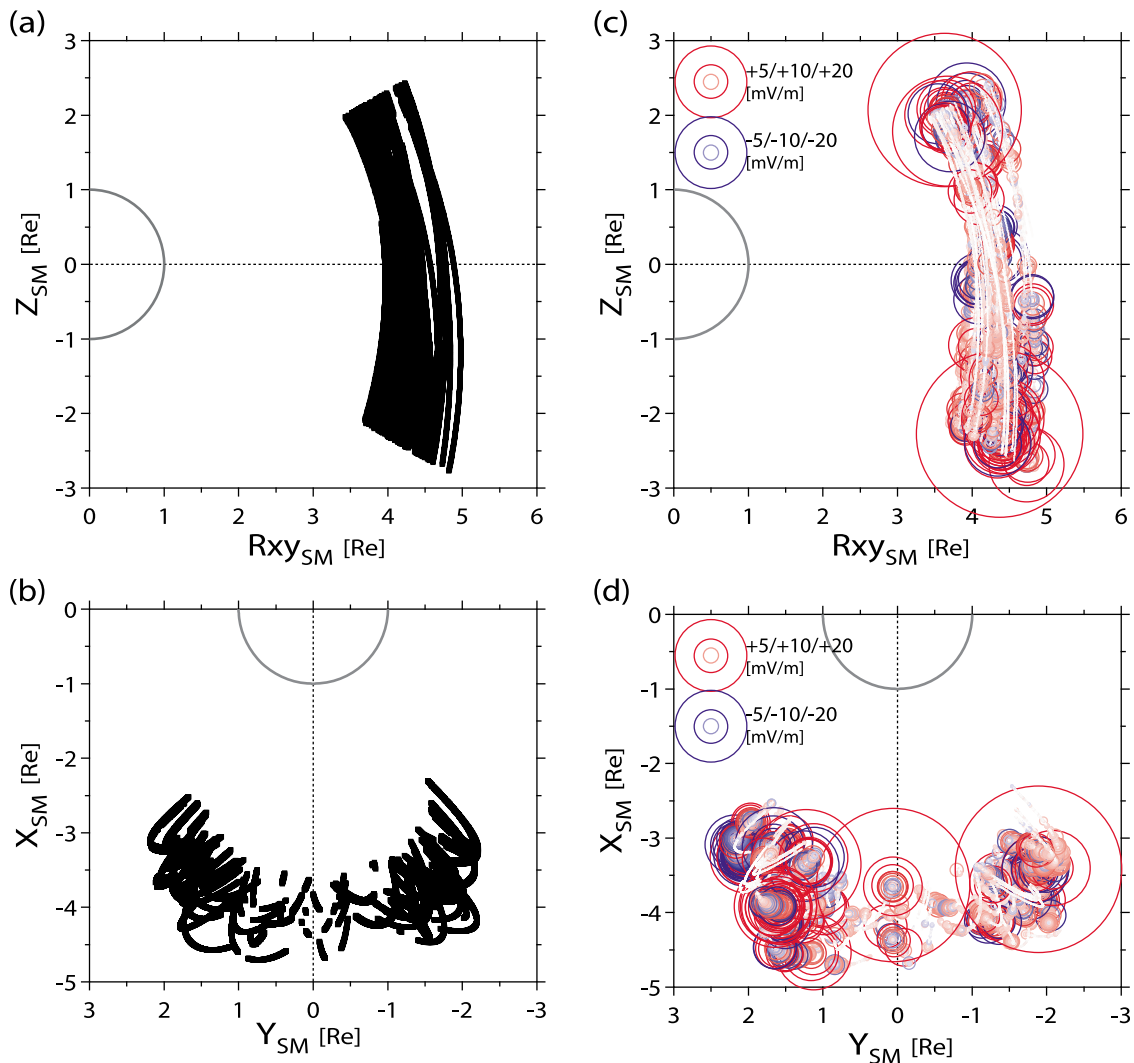


Figure 8. The Cluster positions in the SM (a) meridional and (b) equatorial planes. (c and d) The distribution of E_Y in the same planes. The sign and magnitude of E_Y are presented by the color and size of circles. See text for details.

ment for four consecutive 10 min intervals. For each image, measurements from 2 to 3 different energy channels are combined. The circle at the center is Earth, and dipole field lines at $L = 4$ and 8 are shown at four different local times as marked. The ENA flux is usually most intense at the rim of Earth due to the altitudinal profile of neutral atom density, which increases (double-)exponentially toward the Earth [Brandt *et al.*, 2002; Rairden *et al.*, 1986]. The initial auroral brightening near midnight occurred at 0120 UT in the middle of the first 10 min interval. The ENA flux enhanced subsequently not only at low altitudes but also in the near-Earth region strongly suggesting that the ring current intensified. Clusters 1 and 4 observed the dipolarization between the third and fourth 10 min periods. However, we cannot find any clear enhancement of either low-energy or high-energy hydrogen flux. The oxygen ENA flux enhanced but in the dusk sector not in the dawn sector where Cluster was located. Therefore, the effect of the observed dipolarization on the global ring current population, if at all, was minimal. This is reasonable because the dipolarization itself was localized and its impact

on global geomagnetic activity as measured by auroral emission was also very limited.

4. Statistical Study

[21] In this section we statistically examine the characteristics of electric fields in the nightside inner magnetosphere during geomagnetically active periods. A focus is placed on the occurrence of strong electric fields and their relationship with the change of local magnetic field. We first selected Cluster perigee passes for which $Sym-H$ was continuously less than -25 nT for 4 h centered at the crossing of the geomagnetic equator. A total of 34 events were selected from a 5 year period of 2001–2005. All events took place in January–April because of the precession of satellite orbit. For each event, we then selected intervals for each Cluster satellite when the satellite was within 30° in MLat and within 3 h from midnight in MLT. Finally, the spin average of Cluster EFW data has to meet our quality criteria (section 2). In this part of study we use 20 s (5 spin periods) median

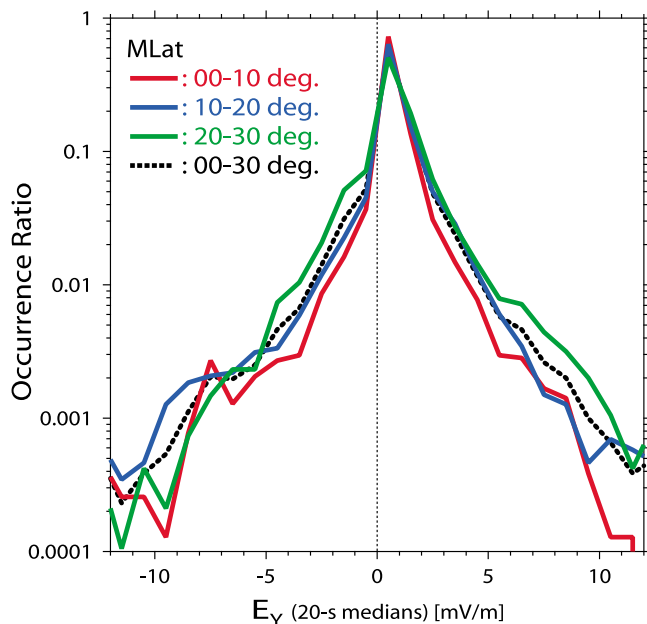


Figure 9. The occurrence ratio of E_Y (20 s medians) for three different ranges of MLat, $0 < |\text{MLat}| \leq 10^\circ$ (red), $10^\circ < |\text{MLat}| \leq 20^\circ$ (blue), and $20^\circ < |\text{MLat}| \leq 30^\circ$ (green), along with that for the entire event set (black dotted line).

values of E_Y . The final data set consists of about 26,000 data points.

[22] Figures 8a and 8b show the satellite position in the meridional and equatorial planes, respectively, in SM coordinates for thus created event set, whereas Figures 8c and 8d show in the same planes the distributions of E_Y with magnitudes larger than 1 mV/m. The sign and magnitude of E_Y are presented by the color and size of circles. As E_Y becomes positively larger exceeding 1 mV/m, the color change from white to red and the diameter becomes larger (data points with E_Y less than 1 mV/m were excluded from Figure 8). In the same way, as E_Y becomes negatively larger, the circle becomes more bluish and larger. It appears that E_Y tends to be larger off the equator (Figure 8c), which will be confirmed next and may be related to the crossing of the boundary layer. Large circles, whether reddish or bluish, are distributed more densely in the premidnight sector than in the postmidnight sector even though the density of measurements is rather symmetric with respect to midnight. In contrast, the circles are distributed far less densely and appear to be smaller in the midnight sector, which at least partially reflects the sparse measurements around midnight (Figure 8b).

[23] Figure 9 shows the occurrence ratio of E_Y for three different ranges of MLat by different colors; that is, $0 < |\text{MLat}| \leq 10^\circ$ (red), $10^\circ < |\text{MLat}| \leq 20^\circ$ (blue), and $20^\circ < |\text{MLat}| \leq 30^\circ$ (green). The black dotted line is for the entire event set. The occurrence ratio is calculated by dividing the number of data points in each bin by the total number of data points. Therefore, the value of occurrence ratio depends on the width of bin, whereas the overall shape does not. In Figure 9 each bin is 1 mV/m wide. There are two important points to make in Figure 9. First, all those distributions are

biased positively as shown by their peak location at $0 < E_Y \leq +1$ mV/m. That is, the average electric field is directed duskward as expected from the normal pattern of magnetospheric convection. Second, although the distributions are not very smooth for large values of $|E_Y|$, E_Y tends to be distributed more widely farther off the equator. In other words, large E_Y is observed more frequently off the equator. The mean and standard deviation of E_Y are (0.55, 1.38), (0.68, 1.76), and (0.76, 2.19) [mV/m] for $0 < |\text{MLat}| \leq 10^\circ$, $10^\circ < |\text{MLat}| \leq 20^\circ$, and $20^\circ < |\text{MLat}| \leq 30^\circ$, respectively, and (0.67, 1.83) for the entire data set. Note that the standard deviation is larger than twice the average.

[24] The issue of primary interest is how/if E_Y is related to the change of local magnetic field, $d(\Delta H)/dt$ and $d|\Delta V|/dt$. Here $d(\Delta H)/dt$ and $d|\Delta V|/dt$ are estimated from 20 s means of magnetic measurements. More specifically, for $d(\Delta H)/dt$ for the 20 s median of E_Y at $t = t_0$ (t_0 is the center of the 20 s time window), we calculated the 20 s means of ΔH , the difference between the measured H component and the corresponding component of the quiet time ($Kp = 0$) T89 model, at $t = t_0 - 10$ s and $t_0 + 10$ s and then divided the difference by 20 s, that is, $(\Delta H(t_0 + 10 \text{ s}) - \Delta H(t_0 - 10 \text{ s}))/20 \text{ s}$. $d|\Delta V|/dt$ is estimated in the same way but using $\Delta|V|$ instead of ΔH . The subtraction of the model field, even if crude, was required because otherwise systematic biases are introduced. For example, because Cluster always crosses the magnetic equator from the Southern to the Northern Hemisphere, the temporal change of $|V|$ is biased negative and positive for data points below and above the magnetic equator, respectively, and those biases are comparable in magnitude to changes associated with phenomena.

[25] Figure 10 shows E_Y in the same format as Figures 8c and 8d but in the frame of $d(\Delta H)/dt$ versus $d|\Delta V|/dt$. When the local magnetic field becomes more dipolar (stretches), ΔH increases (decreases) and $|\Delta V|$ decreases (increases). Therefore, the second quadrant corresponds to depolarization, whereas the fourth quadrant to stretching. Note, however, that $d(\Delta H)/dt$ and $d|\Delta V|/dt$ are based on 20 s dif-

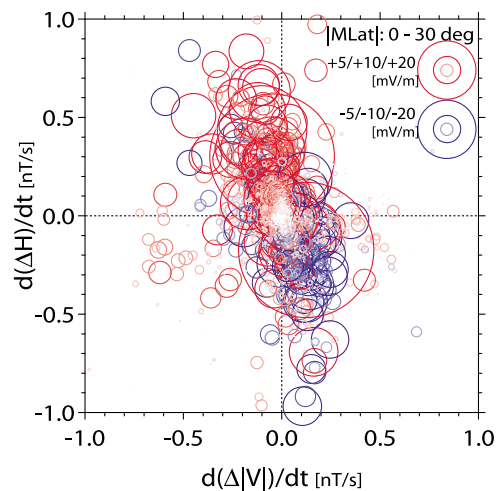


Figure 10. The distribution of E_Y in the frame of $d(\Delta H)/dt$ versus $d|\Delta V|/dt$. The sign and magnitude of E_Y are shown in the same format as Figures 8c and 8d.

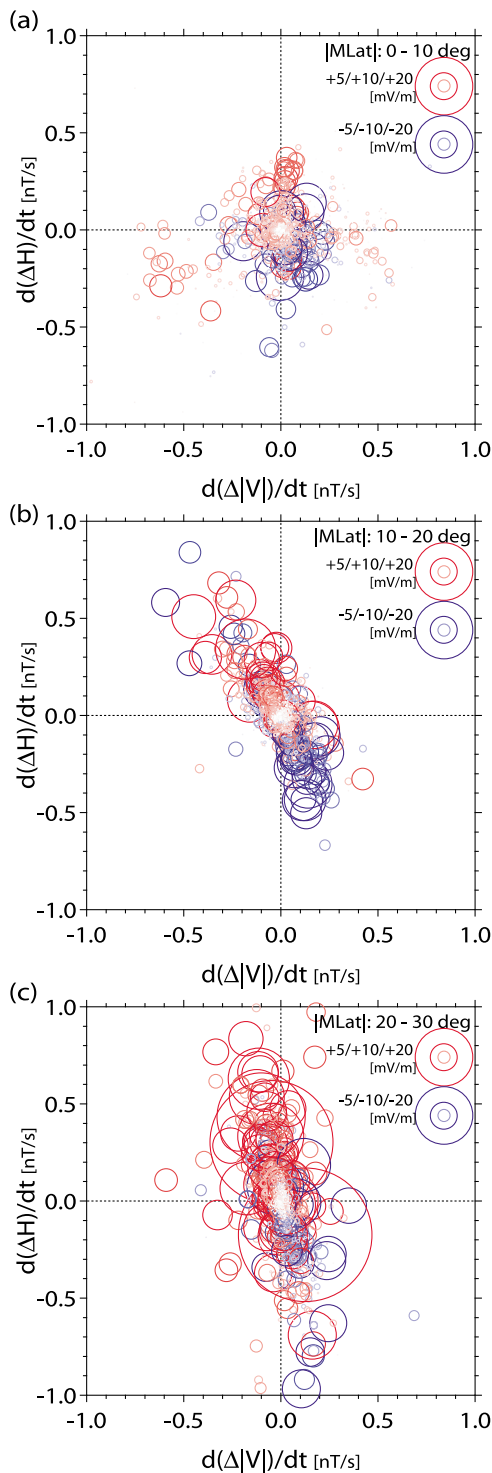


Figure 11. The same as Figure 10 but separately for three different MLat ranges, (a) $0 < |MLat| \leq 10^\circ$, (b) $10^\circ < |MLat| \leq 20^\circ$, and (c) $20^\circ < |MLat| \leq 30^\circ$.

ferentiation, and therefore, magnetic changes to which we are referring as dipolarization and stretching can be more localized in both time and space than one may expect for the configurational change of the magnetotail, and we found that some changes even correspond to ULF waves.

[26] There are two points to note in Figure 10. First, data points are scattered along a direction that extends in the second and fourth quadrants. We also confirmed this tendency with the original data set, which includes data points with $|E_Y| < 1$ mV/m (such points are excluded from Figure 10). This result indicates that magnetic changes, especially large changes, in the meridional plane are well described as dipolarization and stretching. Second and more importantly, the sign of E_Y is well organized by the change of local magnetic field. That is, E_Y tends to be positive (duskward) when the local magnetic field becomes more dipolar, and it tends to be negative (dawnward) when it is stretched. This result strongly suggests that strong electric fields in the inner magnetosphere are mostly inductive.

[27] Figure 11 shows E_Y in the same format as Figure 10 but separately for three different MLat ranges. Some differences can be found among them. Whereas the data points tend to be scattered in a certain orientation at $10^\circ < |MLat| \leq 20^\circ$ (Figure 11b) and $20^\circ < |MLat| \leq 30^\circ$ (Figure 11c), the points are scattered more isotropically at $0 < |MLat| \leq 10^\circ$ (Figure 11a). Nevertheless, also in this equatorial range, the magnetic change is the primary factor that determines the sign of E_Y . That is, E_Y tends to be positive and negative for $d(\Delta H)/dt > 0$ and < 0 , respectively. The different characteristics of E_Y at $0 < |MLat| \leq 10^\circ$ might suggest the occurrence of low-frequency waves with electric field confined near the magnetic equator. In fact, periodic fluctuations of E_Y were observed on some perigee passes, but the characteristics of such waves are the subject of future study. Another interesting feature is the difference in the orientation of data point scatter between $10^\circ < |MLat| \leq 20^\circ$ and $20^\circ < |MLat| \leq 30^\circ$. Magnetic changes are more closely aligned in the H axis at $20^\circ < |MLat| \leq 30^\circ$ than at $10^\circ < |MLat| \leq 20^\circ$, and it tends to be perpendicular to the local magnetic field; at $20^\circ < |MLat| \leq 30^\circ$, the background magnetic field is close to the V axis (not shown). It is possible that when large E_Y is observed farther off the equator, the associated change of current takes place farther down the tail, and therefore, the resultant magnetic perturbation tends to be vertical.

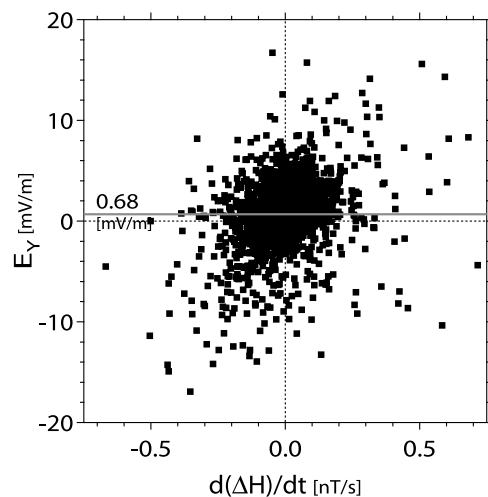


Figure 12. E_Y versus $d(\Delta H)/dt$ for $10^\circ < |MLat| \leq 20^\circ$. The gray horizontal line marks the overall average, 0.68 mV/m.

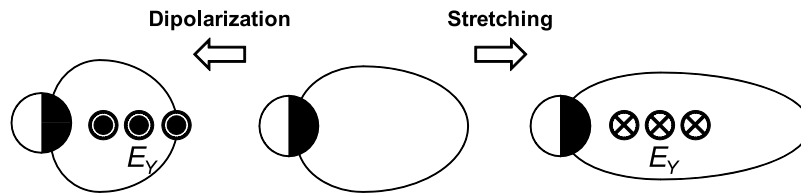


Figure 13. Schematic illustration of inductive electric fields and the change of magnetic configuration in the meridional plane.

[28] Figure 12 shows E_Y as a function of dH/dt for $10^\circ < |MLat| \leq 20^\circ$. Although points are scattered widely, large E_Y tend to be in the first and third quadrants and the overall distribution appears to extend orthogonally, reconfirming that strong electric fields are mostly inductive. Using the slope of the orthogonal line, i.e., 20 mV/m for 0.75 nT/s, for the induction equation, $\nabla \times \vec{E} = -\partial\vec{B}/\partial t$, the spatial scale of E_Y variation in the meridional plane is estimated at $4.2 R_E$. However, as we did a linear regression analysis with the entire data points, we found that the slope of the fitted line is far more gradual than the slope corresponding to the orthogonal line, giving a spatial scale of $0.7 R_E$. This is because points with small E_Y constitute a predominant majority of the data set, and they depend, if at all, very weakly on dH/dt . Presumably, they are electrostatic, rather than inductive. The overall average of E_Y , 0.68 mV/m as marked by the horizontal line in Figure 12, may appear to be small in the figure, but it is actually significant as a statistic electric field (section 1). Therefore, even though we have been paying attention to strong electric fields, we emphasize that the result of this study does not diminish in any sense the importance of electrostatic electric fields in the convection in the inner magnetosphere.

5. Discussion

[29] In this study we used Cluster EFW data acquired within 30° in MLat. As we found for the 18 January event, strong electric fields are often observed at crossings of the plasma sheet boundary layer. Therefore, even though we focused on Cluster perigee passes, the L values of field lines on which strong electric fields were observed cover a wide range. There are, however, two points to make. First, even though the occurrence of strong electric fields is more frequent farther away from the magnetic equator (Figure 9), their characteristics, which we will discuss below, are qualitatively very similar among three 10° -wide MLat ranges we examined. Second, whether or not the spacecraft was in the boundary layer is perhaps less critical for active periods because the ring current region itself is mapped to the ionosphere as a part of the auroral oval. In the 18 January 2005 event, the Cluster footprint was in the auroral oval throughout the interval of highly fluctuating electric fields (Figure 6), and this was also the case for the 18 April 2002 storm event (Paper 1). Therefore, in the following, we will discuss the results of the present study in terms of the dynamics of active time inner magnetosphere in general.

[30] It is well known that the electric field tends to be large in the inner magnetosphere when geomagnetic activity is high (section 1). The average of E_Y measured by Cluster is 0.67 mV/m, which is consistent with the results of the past

studies [e.g., Rowland and Wygant, 1998]. More importantly, the occurrence distribution of E_Y is characterized by its extending tails (Figure 9). The standard deviation is more than twice the average of E_Y , and E_Y often becomes even negative. This characteristic of E_Y is akin to that of the flow velocity in the plasma sheet, which is bursty at storm time [Hori *et al.*, 2005; Ohtani and Mukai, 2008] as well as nonstorm time [e.g., Angelopoulos *et al.*, 1992]. Note, however, that the velocity of the electric drift in the inner magnetosphere is smaller than that of the plasma sheet flow by more than an order of magnitude. It is only 33 km/s for an electric field of 10 mV/m and a total magnetic field of 300 nT, whereas the velocity of the plasma sheet flow often reaches several hundred kilometers per second and higher.

[31] The magnetic configuration of the inner magnetosphere is more stable than that of the plasma sheet. For example, the equatorial magnetic field does not become southward in the inner magnetosphere. Because of the strong background field, the magnetic inclination may not change significantly even if the change of local magnetic field is large in magnitude. This explains, at least partially, why the occurrence frequency of dipolarization is very low in the inner magnetosphere [e.g., Lopez *et al.*, 1988] if dipolarization is identified based on the change of magnetic inclination.

[32] However, it is the magnetic change, not the change of magnetic inclination, which determines the inductive electric field. In the 18 January 2005 event the H component increased by 50 nT in association with the dipolarization at 0145 UT (Figure 5a). It should therefore be reasonable that the associated inductive electric field is also unusually large. The spin (4 s) average E_Y reached 20 mV/m in that event, and the statistical study shows that the 20 s median of $|E_Y|$ often exceeds 5 mV/m. Conversely, when large E_Y is observed, the associated magnetic change tends to be large (Figures 10–12). We therefore conclude that large E_Y in the inner magnetosphere is mostly inductive. That is, as we found in the present study and is schematically shown in Figure 13, the electric field is directed duskward when the local magnetic configuration becomes more dipolar, whereas it is directed downward when the local magnetic configuration gets stretched, and its magnitude is determined by the rate of magnetic change. Strong dawn-to-dusk electric fields are observed in the plasma sheet at local dipolarization [e.g., Aggson *et al.*, 1983; Fairfield *et al.*, 1998], and here again we see a similarity between the active time inner magnetosphere and plasma sheet.

[33] For large E_Y we estimated from the induction equation that the typical spatial scale of E_Y is $4.2 R_E$. Note that this estimate is based on the assumption that $\partial E_Y/\partial x$ is dominant in the Z component of $\nabla \times \vec{E}$ (here we are using the H

magnetic component as a proxy of B_Z). For the dipolarization at 0145 UT on 18 January 2005, Cluster 1 observed the H component to increase by 40 nT in 25 s and a peak E_Y of 20 mV/m, which gives a spatial scale of $2.0 R_E$. However, Cluster 4, which was located at (630, 550, -490) km from Cluster 1 in SM coordinates, observed a very similar dipolarization signature but with a 30 s delay (Figure 4). This time delay is comparable to the duration of the sharp H increase. Therefore, if the dipolarization signature was propagating, its spatial scale must be comparable to the separation between Clusters 1 and 4. From the estimated propagation velocity, 30 km/s (section 3), the radial scale is estimated at 900 km, which is significantly shorter than $2.0 R_E$. This apparent discrepancy may suggest that the aforementioned assumption does not hold in this case and that the associated spatial structure is complex. In fact, the global auroral image shows that active regions were patchy around the Cluster footprint. It is also possible that the electric field was partially electrostatic and the electrostatic part was also confined around the time of dipolarization. In general, if dipolarization is accompanied by the formation of a 3-D current system, i.e., substorm wedge current system, a part of the magnetospheric electric field needs to be mapped to the ionosphere along the magnetic field line, and such an electric field has to be electrostatic.

[34] Although strong electric fields are well organized by the change of local magnetic field, this does not mean that all such events are the same phenomenon. In the 18 January 2005 event, large E_Y was observed first in association with the satellite crossing of the boundary layer and then at 0145 UT when the local magnetic field sharply became dipolar. For each interval we found that E_Y was well correlated with the change of the H component. The dipolarization at 0145 UT took place during the recovery of the preceding activity, and it did not make any significant impact on the global auroral activity (Figure 6) or on the global distribution of the ENA emission (Figure 7), which is consistent with the fact that the dipolarization and large E_Y were spatially limited in the inner magnetosphere. Dipolarization was also observed by Cluster on a perigee pass in the 18 April 2002 storm event. In that event, in contrast, all four Cluster satellites observed in the premidnight ring current similar magnetic variations and strong electric fields that were well correlated with them [Paper 1]. Whereas in that event the separation among the four Cluster satellites was much smaller, a few hundred kilometers at maximum, the GOES 10 geosynchronous satellite simultaneously observed dipolarization a few R_E outside of Cluster. Considering that this dipolarization event corresponded to one of the sawtooth injections, which are known to be global [e.g., Clauer *et al.*, 2006], it is reasonable that satellite observations were coherent. However, it would be rather difficult to infer from the local observation in the inner magnetosphere whether the corresponding event is globally coherent as was observed in the 18 April 2002 event or it is spatially localized as was observed in the 18 January 2005 event.

[35] It is also worth commenting the time scale of magnetic variations. In the 18 January 2005 event, the time scale of the dipolarization at 0145 UT was about 1 min, and the sharpest H increase occurred in 25 s. A similar time scale was also found for the dipolarization event of the 18 April 2002 event [Paper 1]. In contrast, the typical duration of the

substorm growth phase is longer by more than an order of magnitude. Nevertheless, as we found in Figures 10 and 11, there is no clear difference in $d(\Delta H)/dt$ or $d|\Delta V|/dt$ between dipolarization and stretching (points are scattered along a certain orientation without any clear break at the origin). However, at the rate of 0.25 nT/s, for example, the magnetic field changes 150 nT in 10 min, and the associated magnetic change would become comparable to, or would even exceed, the background magnetic field for the typical duration of the substorm growth phase, say 30 min, which is very unlikely in the inner magnetosphere. Although these facts imply, and we confirmed (not shown), that the stretching of local magnetic field associated with strong dusk-to-dawn electric fields is also localized in time, the responsible process is an open question.

[36] Finally, it would be useful to address the present result in the context of the storm-substorm relationship. The storm-substorm relationship is usually addressed in terms of the contribution of substorm injection to the ring current intensification. However, the difficulty of this idea is that energetic ions drift duskward after injection because of magnetic gradient and field line curvature. Such ions may contribute to the formation of the partial ring current in the dusk sector, but the effect of each injection is temporary. In contrast, if the region of injection, that is, the region of strong electric fields extends earthward into the ring current area where drift orbits are closed in the magnetosphere, the associated injection would bring plasma sheet ions most efficiently to the ring current and energize them. Or, if substorm-like processes take place inside the ring current, the associated electric field can energize ring current ions locally. The result of the present study indicates that substorm-like processes take place inside the ring current, and they efficiently intensify the ring current. The role of such processes in the ring current intensification remains to be addressed quantitatively, for which it would be essential to treat strong electric fields consistently with time-varying magnetic configurations.

6. Summary

[37] Using Cluster electric field and magnetic field data on perigee passes, we examined the characteristics of electric fields in the inner magnetosphere. First, we examined the storm event of 18 January 2005, during which Cluster crossed the magnetic equator at MLT \sim 03. Off the equator Cluster observed large (>10 mV/m) fluctuations of E_Y in association with the crossing of the boundary layer, and closer to the equator two Cluster satellites, Clusters 1 and 4, observed dipolarization with a large (>50 nT) increase in H and a 20 mV/m spike of E_Y . Guided by this event study, we statistically examined the characteristics of E_Y focusing on the nightside ($21 \leq \text{MLT} \leq 03$) low-latitude ($|\text{IMLat}| \leq 30^\circ$) region during geomagnetically active ($Sym-H < -25$ nT for 4 h) periods. We found that E_Y tends to be large in magnitude in the premidnight sector presumably corresponding to the more frequent occurrence of substorms. E_Y also tends to be larger off the equator than near the equator. The overall average of E_Y is 0.67 mV/m, which reflects the enhancement of convection electric field at geomagnetically active time. However, the occurrence distribution of E_Y has extending tails with a standard deviation larger than twice the average value of E_Y , and $|E_Y|$ occasionally exceeds 5 mV/m. Fur-

thermore, we found that such strong electric fields are well organized by the change of local magnetic field. When the local magnetic configuration becomes more dipolar, E_Y tends to be positive (duskward), whereas it tends to be negative (dawnward) when the configuration becomes more stretched. The magnitude of E_Y tends to be proportional to the change of the H magnetic component.

[38] We therefore concluded that those strong electric fields are mostly inductive. From the induction equation the typical spatial scale of E_Y is estimated at $4.2 R_E$. We, however, emphasize that the corresponding process/phenomenon can be different from event to event. Some events may be globally coherent as was reported previously for the 18 April 2002 event. In other events such as the 18 January 2005 event, a strong electric field was so confined in space that even nearby Cluster satellites did not observe similar signatures. Nevertheless, in general, those strong electric fields locally interact with ring current ions, and therefore, they may play a critical role in the storm time ring current formation. The present study also provides a new perspective about storm-substorm relationship. That is, if substorm (-like) processes take place inside the ring current, it is possible that they intensify the ring current more effectively than injecting energetic particles from outside of the ring current.

[39] **Acknowledgments.** The Cluster EFW data were provided by M. Andre through the Cluster Active Archive (CAA). We are most grateful to C. Cully for his kind advice for using the EFW data. The Cluster fluxgate magnetometer data were provided by E. Lucek through CAA. The *Sym-H* index was provided by T. Iyemori through the World Data Center for Geomagnetism, Kyoto. The ACE/MFI and Solar Wind Electron Proton Alpha Monitor data sets were provided by C. W. Smith and D. J. McComas, respectively, through NASA/CDAWeb. Work at Johns Hopkins University Applied Physics Laboratory was supported by NASA grants NNX07AG07G and NNX09AF46G.

[40] Masaki Fujimoto thanks the reviewers for their assistance in evaluating 2010ja015745.

References

- Aggson, T., J. Heppner, and N. Maynard (1983), Observations of large magnetospheric electric fields during the onset phase of a substorm, *J. Geophys. Res.*, *88*(A5), 3981–3990, doi:10.1029/JA088iA05p03981.
- Angelopoulos, V., W. Baumjohann, C. F. Kennel, F. V. Coroniti, M. G. Kivelson, R. Pellat, R. J. Walker, H. Lühr, and G. Paschmann (1992), Bursty bulk flows in the inner central plasma sheet, *J. Geophys. Res.*, *97*(A4), 4027–4039, doi:10.1029/91JA02701.
- Balogh, A., et al. (2001), The Cluster magnetic field investigation: Overview of inflight performance and initial results, *Ann. Geophys.*, *19*, 1207–1217.
- Brandt, P. C., R. Demajistre, E. C. Roelof, S. Ohtani, D. G. Mitchell, and S. Mende (2002), IMAGE/high-energy energetic neutral atom: Global energetic neutral atom imaging of the plasma sheet and ring current during substorms, *J. Geophys. Res.*, *107*(A12), 1454, doi:10.1029/2002JA009307.
- Burch, J. L. (2000), IMAGE mission overview, *Space Sci. Rev.*, *91*(1–2), 1–14.
- Chen, M. W., L. R. Lyons, and M. Schulz (1994), Simulations of phase space distributions of storm time proton ring current, *J. Geophys. Res.*, *99*(A4), 5745–5759, doi:10.1029/93JA02771.
- Clauer, C. R., X. Cai, D. Welling, A. DeJong, and M. G. Henderson (2006), Characterizing the 18 April 2002 storm time sawtooth events using ground magnetic data, *J. Geophys. Res.*, *111*, A04S90, doi:10.1029/2005JA01099.
- Daglis, I. A., R. M. Thorne, W. Baumjohann, and S. Orsini (1999), The terrestrial ring current: Origin, formation, and decay, *Rev. Geophys.*, *37*(4), 407–438, doi:10.1029/1999RG900009.
- Ebihara, Y., and M. Ejiri (2003), Numerical simulation of the ring current: Review, *Space Sci. Rev.*, *105*(1–2), 377–452.
- Escoubet, C. P., M. Fehringer, and M. Goldstein (2001), The Cluster mission, *Ann. Geophys.*, *19*, 1197–1200.
- Fairfield, D. H., et al. (1998), Geotail observations of substorm onset in the inner magnetotail, *J. Geophys. Res.*, *103*(A1), 103–117, doi:10.1029/97JA02043.
- Fok, M.-C., T. E. Moore, and D. C. Delcourt (1999), Modeling of inner plasma sheet and ring current during substorms, *J. Geophys. Res.*, *104*(A7), 14,557–14,569, doi:10.1029/1999JA900014.
- Fok, M.-I., T. E. Moore, and M. E. Greenspan (1996), Ring current development during storm main phase, *J. Geophys. Res.*, *101*(A7), 15,311–15,322, doi:10.1029/96JA01274.
- Gonzalez, W. D., J. A. Joselyn, Y. Kamide, H. W. Kroehl, G. Rostoker, B. T. Tsurutani, and V. M. Vasylunas (1994), What is a geomagnetic storm?, *J. Geophys. Res.*, *99*(A4), 5771–5792, doi:10.1029/93JA02867.
- Gustafsson, G., et al. (2001), First results of electric field and density observations by Cluster EFW based on initial months of operation, *Ann. Geophys.*, *19*, 1219–1240.
- Hori, T., A. T. Y. Lui, S. Ohtani, P. C. Son Brandt, B. H. Mauk, R. W. McEntire, K. Maezawa, T. Mukai, Y. Kasaba, and H. Hayakawa (2005), Storm time convection electric field in the near-Earth plasma sheet, *J. Geophys. Res.*, *110*, A04213, doi:10.1029/2004JA010449.
- Kamide, Y., et al. (1998), Current understanding of magnetic storms: Storm-substorm relationships, *J. Geophys. Res.*, *103*(A8), 17,705–17,728, doi:10.1029/98JA01426.
- Keika, K., et al. (2009), Substorm expansion triggered by a sudden impulse front propagating from the dayside magnetopause, *J. Geophys. Res.*, *114*, A00C24, doi:10.1029/2008JA013445.
- Lopez, R. E., A. T. Y. Lui, D. G. Sibeck, R. W. McEntire, L. J. Zanetti, T. A. Potemra, and S. M. Krimigis (1988), The longitudinal and radial distribution of magnetic reconfigurations in the near-Earth magnetotail as observed by AMPTE/CCE, *J. Geophys. Res.*, *93*(A2), 997–1001, doi:10.1029/JA093iA02p00997.
- Lyons, L. R., D.-Y. Lee, C.-P. Wang, and S. B. Mende (2005), Global auroral responses to abrupt solar wind changes: Dynamic pressure, substorm, and null events, *J. Geophys. Res.*, *110*, A08208, doi:10.1029/2005JA011089.
- Maynard, N., T. Aggson, and J. Heppner (1983), The plasmaspheric electric field as measured by ISEE 1, *J. Geophys. Res.*, *88*(A5), 3991–4003, doi:10.1029/JA088iA05p03991.
- McComas, D. J., S. J. Bame, P. Barker, W. C. Feldman, J. L. Phillips, P. Riley, and J. W. Griffée (1998), Solar Wind Electron Proton Alpha Monitor (SWEPAM) for the Advanced Composition Explorer, *Space Sci. Rev.*, *86*, 563–612.
- McPherron, R. L. (1997), The role of substorms in the generation of magnetic storms, in *Magnetic Storms*, edited by B. T. Tsurutani et al., p. 131, AGU, Washington, D. C.
- Mende, S. B., et al. (2000), Far ultraviolet imaging from the IMAGE spacecraft: 2. Wideband FUV imaging, *Space Sci. Rev.*, *91*, 271–285.
- Mitchell, D. G., et al. (2000), High energy neutral atom (HENA) imager for the Image mission, *Space Sci. Rev.*, *91*, 67–112.
- Nishimura, Y., A. Shinbori, T. Ono, M. Iizima, and A. Kumamoto (2006), Storm time electric field distribution in the inner magnetosphere, *Geophys. Res. Lett.*, *33*, L22102, doi:10.1029/2006GL027510.
- Ohtani, S., and T. Mukai (2008), Statistical characteristics of the storm time plasma sheet, *J. Geophys. Res.*, *113*, A01221, doi:10.1029/2007JA012547.
- Ohtani, S., M. Nosé, G. Rostoker, H. Singer, A. T. Y. Lui, and M. Nakamura (2001), Storm-substorm relationship: Contribution of the tail current to Dst, *J. Geophys. Res.*, *106*(A10), 21,199–21,209, doi:10.1029/2000JA000400.
- Ohtani, S., et al. (2007), Cluster observations in the inner magnetosphere during the 18 April 2002 sawtooth event: Dipolarization and injection at $r = 4.6 R_E$, *J. Geophys. Res.*, *112*, A08213, doi:10.1029/2007JA012357.
- Rairden, R. L., L. A. Frank, and J. D. Craven (1986), Geocoronal imaging with Dynamic Explorer, *J. Geophys. Res.*, *91*(A12), 13,613–13,630, doi:10.1029/JA091iA12p13613.
- Reiff, P. H., R. W. Spiro, and T. W. Hill (1981), Dependence of polar cap potential drop on interplanetary parameters, *J. Geophys. Res.*, *86*(A9), 7639–7648, doi:10.1029/JA086iA09p07639.
- Rowland, D. E., and J. R. Wygant (1998), Dependence of the large-scale, inner magnetospheric electric field on geomagnetic activity, *J. Geophys. Res.*, *103*(A7), 14,959–14,964, doi:10.1029/97JA03524.
- Shepherd, S. G., R. A. Greenwald, and J. M. Ruohoniemi (2002), Cross polar cap potentials measured with Super Dual Auroral Radar Network during quasi-steady solar wind and interplanetary magnetic field conditions, *J. Geophys. Res.*, *107*(A7), 1094, doi:10.1029/2001JA000152.
- Shue, J.-H., P. T. Newell, K. Liou, C. Meng, Y. Kamide, and R. P. Lepping (2002), Two-component auroras, *Geophys. Res. Lett.*, *29*(10), 1379, doi:10.1029/2002GL014657.

- Smith, C. W., M. H. Acuna, L. F. Burlaga, J. L'Heureux, N. F. Ness, and J. Scheifele (1998), The ACE magnetic fields experiment, *Space Sci. Rev.*, *86*, 613–632.
- Tsyganenko, N. A. (1989), A magnetospheric magnetic field model with the warped tail current sheet, *Planet. Space Sci.*, *37*, 5–20.
- Tsyganenko, N. A. (1996), Effects of the solar wind conditions on the global magnetospheric configuration as deduced from data-based field models, in *Proceedings of 3rd International Conference on Substorms (ICS-3)*, *Eur. Space Agency Spec. Publ., ESA SP-389*, 181–185.
- Wolf, R. A., J. W. Freeman, B. A. Hausman, and R. W. Spiro (1997), Modeling convection effects in magnetic storms, in *Magnetic Storms*, edited by B. T. Tsurutani et al., p. 161, AGU, Washington, D. C.
- Wygant, J., D. Rowland, H. Singer, M. Temerin, F. Mozer, and M. Hudson (1998), Experimental evidence on the role of the large spatial scale electric field in creating the ring current, *J. Geophys. Res.*, *103*(A12), 29,527–29,544, doi:10.1029/98JA01436.
- Zhou, X., and B. Tsurutani (2001), Interplanetary shock triggering of night-side geomagnetic activity: Substorms, pseudobreakups, and quiescent events, *J. Geophys. Res.*, *106*(A9), 18,957–18,967, doi:10.1029/2000JA003028.
-
- P. C. Brandt, H. Korth, S. Ohtani, and Y. Zheng, Johns Hopkins University Applied Physics Laboratory, 11100 Johns Hopkins Rd., Laurel, MD 20723, USA. (ohtani@jhuapl.edu)
- K. Keika, Center for Solar-Terrestrial Research, New Jersey Institute of Technology, 323 Martin Luther King Blvd., Newark, NJ 07102, USA.
- S. B. Mende, Space Sciences Laboratory, University of California, 7 Gauss Way, Berkeley, CA 94720, USA.